iScience

CellPress
OPEN ACCESS

Article

Regeneration of interfacial bonding force of waste carbon fibers by light: Process demonstration and atomic level analysis

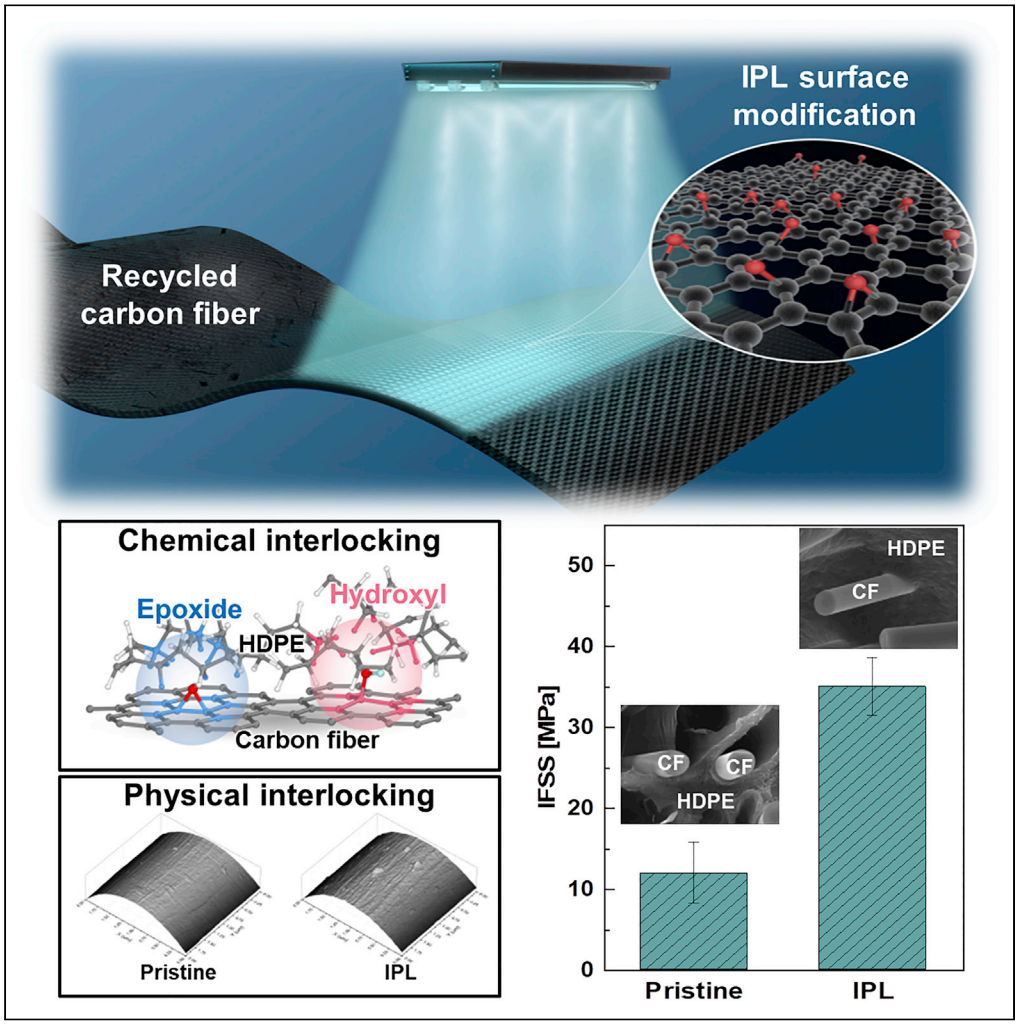

Myounghun Kim, Byeonghwa Goh, Jungpil Kim, Kwang-Seok Kim, Joonmyung Choi

ore21@kitech.re.kr (K.-S.K.)
joonchoi@hanyang.ac.kr (J.C.)

Highlights

IPL irradiation was utilized for surface modification to control HDPE/rCF interfaces

The IPL-irradiated rCF showed an increase in oxygen functional groups and roughness

MD simulation revealed IFSS was enhanced by chemical interaction and interlocking

Surface treatment using IPL energy facilitates commercialization of rCF composites

Kim et al., iScience 25, 105367
November 18, 2022
https://doi.org/10.1016/j.isci.2022.105367

iScience

CellPress
OPEN ACCESS

Article

Regeneration of interfacial bonding force of waste carbon fibers by light: Process demonstration and atomic level analysis

Myounghun Kim,[1,4] Byeonghwa Goh,[2,3,4] Jungpil Kim,[1] Kwang-Seok Kim,[1,5,*] and Joonmyung Choi[2,3,*]

SUMMARY

Although interest in recycling carbon fibers is rapidly growing, practical applications of recycled carbon fibers (rCFs) are limited owing to their poor wettability and adhesion. Surface modification of CFs was achieved through intense pulsed light (IPL) irradiation, which functionalizes surface of rCFs. Surface energy, chemical composition, morphology, and interfacial shear strength (IFSS) of rCFs before and after IPL irradiation were investigated. The rCF IPL-irradiated at 1,200 V improved both polar and dispersive components of surface energy, and the IFSS significantly increased by 2.93 times in relation to that of the pristine rCF and reached 95% of that of high-grade commercial CFs. We proposed a mechanism by which oxygen functional groups on the rCF surface enhance the molecular bonding force with HDPE, and the model was validated from molecular dynamics simulations. IPL irradiation is a rapid and effective surface treatment method that can be employed for the manufacture of rCF-reinforced composites.

INTRODUCTION

Carbon fibers (CFs) exhibit excellent mechanical, chemical, and physical properties, such as high tensile strength, wear resistance, corrosion resistance, and electrical and thermal conductivity; thus, they can be widely applied in various industries, including the automotive, aerospace, construction, and ocean industries (Jacob, 2014; Soutis, 2005; Błażejewski et al., 2018; Holmes, 2018; Caltagirone et al., 2021; Meng et al., 2017; Xiong et al., 2021; Cai et al., 2019; Wang et al., 2019). However, CFs have two major disadvantages that prevent them from being used commercially, namely their high cost compared to glass fiber, and poor wettability and adhesion owing to its highly crystalline graphitic surface structure (Chukov et al., 2015; Kim et al., 2011; Yao et al., 2018).

Recycled carbon fibers (rCFs) are a promising alternative to pristine CFs in composite materials (Yao et al., 2018). rCFs, including those that are discarded owing to their underperformance during the manufacturing process or those extracted from CF-reinforced plastic products, are inferior to commercial CFs in terms of their properties; however, they are cheaper and can be used to reinforce polymers. In addition, rCFs are economically and environmentally advantageous because they can be directly reused through recycling (McNally et al., 2008; Kouparitsas et al., 2002). Another remedy involves improving the interfacial adhesion between the CFs and the polymer matrix by modifying the surface of the CFs. The key is to explore physicochemical treatments that substantially enhance the interfacial bonding force between CF and the polymer matrix. The interfacial bonding force refers to the resistance applied to the surfaces of two adjacent materials against external peeling deformation. Experimentally, the characteristics can be evaluated from the interfacial shear strength and the microstructure of the fracture surface. Increasing the effective adhesion area of the interfacial region in the manufacturing process of composite materials thus can be a typical strategy from a macroscopic point of view to improve the properties. More fundamentally, it is also required to devise a strategy to increase the chemical bonding force between atoms placed at the interface at the nanometer scale. Various surface modification methods have been investigated, such as chemical or electrochemical (Pittaman et al., 1997; Zhang et al., 2008; Servinis et al., 2017; Jiang et al., 2014), heat (Cai et al., 2019; Dai et al., 2011), electron beam (Kim et al., 2011), plasma (Jang, 1992; Xie et al., 2011; Yu et al., 2020; Jang and Yang, 2000), and UV/ozone treatment (Osbeck et al., 2011; Rich et al., 2013). These methods result in enhanced interfacial bonding force to the polymer matrix by increasing the surface energy, introducing active functional groups, and increasing the surface roughness.

[1]Carbon & Light Materials Application R&D Group, Korea Institute of Industrial Technology, 222 Palbok-ro, Deokjin-gu, Jeonju 54853, Republic of Korea

[2]Department of Mechanical Design and Engineering, Hanyang University, 222 Wangsimni-ro, Seongdong-gu, Seoul 04763, Republic of Korea

[3]Department of Mechanical Engineering, BK21 FOUR ERICA-ACE Center, Hanyang University, 55 Hanyangdaehak-ro, Sangnok-gu, Ansan 15588, Republic of Korea

[4]These authors contributed equally

[5]Lead contact

*Correspondence: ore21@kitech.re.kr (K.-S.K.), joonchoi@hanyang.ac.kr (J.C.)

https://doi.org/10.1016/j.isci.2022.105367

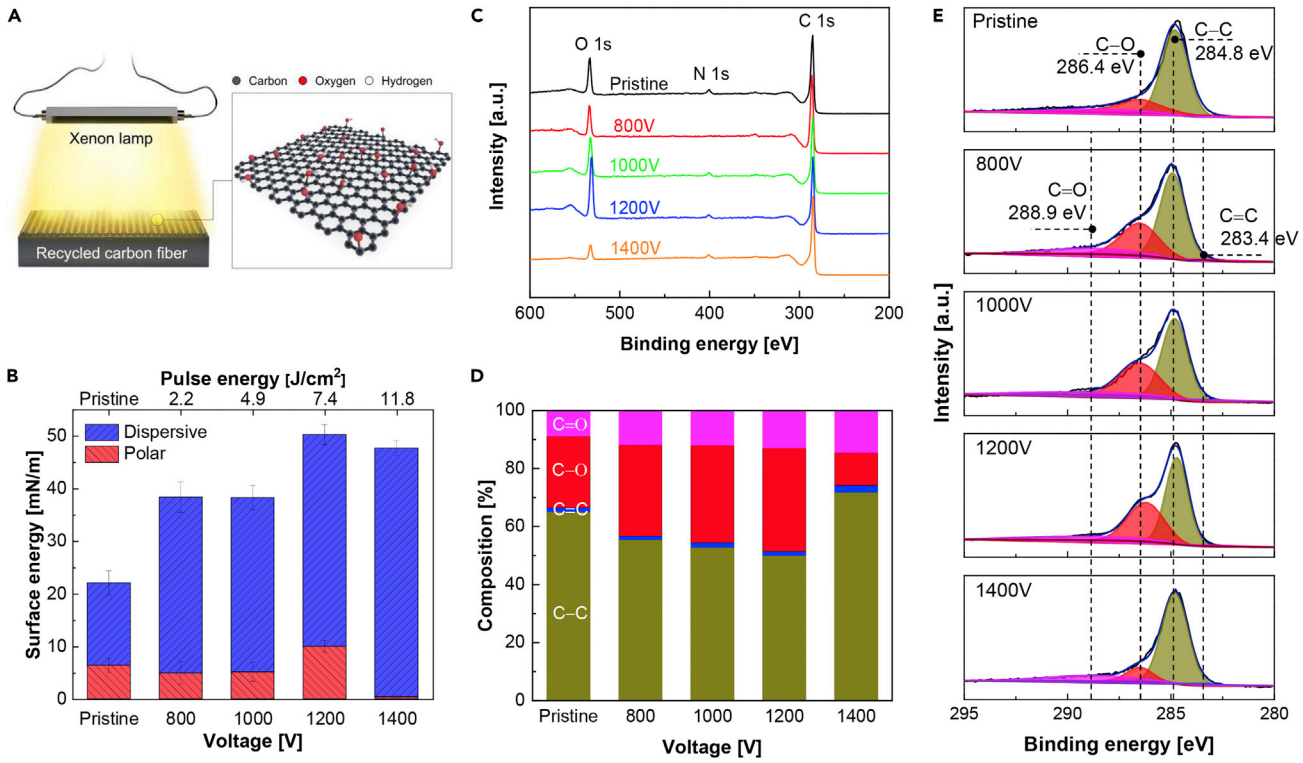

Figure 1. Changes in surface energy and chemical bonds of rCFs before and after IPL irradiation

(A) Schematic diagram of functionalization of the rCF surface using the IPL system.

(B) Total, polar and dispersive surface energies of rCFs IPL-irradiated at various voltages.

(C–E) XPS results of IPL-irradiated rCFs at various voltages; (C) wide-scan spectra, (D) fraction of chemical bond at C 1s spectra and (E) C 1s spectra.

Intense pulsed light (IPL) is a technology that applies light energy in a short period of time using flash lamps. Focus on IPL has continuously increased owing to its advantages, such as simplicity of the process, short process time, selective treatment, and small number of by-products. It has been mainly used in medical applications, printed electronics, and as a substitute for heat treatment (Bitter, 2000; Babilas et al., 2010; Kim et al., 2009; Kang et al., 2011; Jiu et al., 2012; Youn et al., 2018). Recently, surface modification experiments have been conducted, for example, to reduce graphene oxide or improve the adhesion of CF-reinforced plastics (Al-Hamry et al., 2016; Pei and Li, 2017; Kim et al., 2021). However, there have been only few studies on the functionalization of CFs via IPL irradiation (Lee et al., 2017).

The objective of this work is to establish a bridgehead for the commercialization of composite materials using rCFs. To the best of our knowledge, we report the application of IPL irradiation to rCFs, for the first time, to control their surface energy and enhance the mechanical properties of rCF-based composites. The effect of IPL energy on the high-density polyethylene (HDPE)/rCF interface was investigated via both experiments and computational simulations. The physical and chemical modifications, including those of surface energy, surface morphology, surface chemical composition, interfacial adhesion, and mechanical properties, induced by IPL irradiation were first experimentally examined. In addition, a pull-out molecular dynamics (MD) simulation was carried out to analytically examine the underlying mechanism affecting the interfacial mechanical properties of HDPE/rCF composites.

RESULTS

Effects of IPL irradiation on surface characteristics of rCFs

Desized rCFs (Figure S1) were chopped to 6-mm size and then exposed to IPL irradiation, as shown in Figure 1A. To investigate the effects of IPL irradiation on the rCF surface energy, the surface energies of the rCFs, which were IPL-irradiated with various voltages, were calculated from the contact angles of the rCFs against water or diiodomethane (Figure S2), as shown in Figure 1B. As compared with the

Table 1. Surface chemical composition and atomic ratio of rCFs IPL-irradiated at various voltages

	Pristine	800 V	1,000 V	1,200 V	1,400 V
C 1s (at.%)	83.2	80.23	72.31	71.55	87.52
O 1s (at.%)	13.1	14.77	17.75	25.54	6.62
O 1s/C 1s	0.157	0.184	0.245	0.357	0.076

pristine rCF, the surface energies of rCFs irradiated with IPL at 800 and 1,000 V increased from 22.2 to approximately 38.3 mN/m. At 1,200 V, it showed the highest surface energy of 50.3 mN/m, and at 1,400 V, it increased by 2.15 times compared with the pristine rCF, despite a decrease of 5.16% compared with that at 1,200 V, within the error range. Particularly, the polar component showed significantly interesting results depending on the voltage applied. At 800 and 1,000 V, the surface energy was similar to the pristine rCF, and at 1,200 V, the value increased to 10.0 mN/m, which was 56% higher than that of the pristine rCF; however, at 1,400 V, it decreased remarkably to 0.4 mN/m. The IPL irradiation effectively enhanced both dispersive and polar components of the surface energy, and the total energy may be saturated owing to the increased dependence on the dispersive component at voltages above 1,400 V. To a large extent, the increase in the surface energy of the rCFs improved the wettability between the rCFs and the polymer matrix; particularly, the polar functional groups containing oxygen on the rCF surface induced stronger interfacial bonding with the HDPE resin (Jiang et al., 2014; Xie et al., 2011). The surfaces of the IPL-irradiated rCFs were analyzed in terms of their chemical and physical properties to demonstrate their surface energy.

The XPS wide-scan spectra of the IPL-irradiated rCFs presented prominent carbon and oxygen peaks in the binding energy range of 280–298 eV and 525–545 eV, respectively, as shown in Figure 1C. The O 1s peaks became evidently sharper as the voltage increased up to 1,200 V, and their intensity increased; however, subsequently, they decreased at a voltage of 1,400 V. The surface chemical composition and O 1s/C 1s ratio of the rCFs are listed in Table 1. The O 1s/C 1s ratio also increased from 0.157 to 0.357, when the voltage was increased to 1,200 V compared to that of the pristine rCF, and then decreased remarkably to 0.076 at 1,400 V; this trend was similar to that of the polar component of the surface energy (Figure 1B). The increase in the O 1s/C 1s ratio indicates that oxygen-containing polar groups were introduced on the rCF surface through IPL irradiation (Xie et al., 2011). The minimum O 1s/C 1s ratio of 0.076 after an IPL irradiation at 1,400 V was obtained with the highest carbon content and the lowest oxygen content. Low-intensity N 1s peaks were observed in the XPS wide-scan spectra. Further details on the N 1s peaks can be found in the supplementary information (Figure S3).

The deconvolution results of the C 1s peaks show C=C (283.4 eV), C–C (284.8 eV), C–O (286.4 eV), and C=O (288.9 eV) bonds, as shown in Figures 1D and 1E. Overall, the C=O and C=C bonds increased slightly when the voltage increased. The notable result was that the C–O bond on the rCF surfaces increased by approximately 36.1% after IPL irradiation at voltages lower than 1,200 V; however, this bond decreased by 54.3% after IPL irradiation at 1,400 V, compared to that on the pristine rCF. It was surmised that the C–O and C=O bonds dominantly contributed to the presence of the oxygen functional groups, thereby resulting in an increase in the surface energy of the rCFs as well as the surface energy components. At IPL energies above 1,400 V, the remarkable decrease in the O 1s/C 1s ratio was attributed to deoxygenation, which broke the chemical bond between carbon and oxygen on the surface of the rCFs by IPL irradiation (Al-Hamry et al., 2016; Pei and Li, 2017). Besides the voltage, the atmosphere also affects the functionalization of the rCF surface: IPL irradiation under a mixture argon and oxygen more effectively generates oxygen functional groups when compared with irradiation under only argon (Figure S4 and Table S1). The surface energy of the IPL-irradiated rCF decreased by less than 10% for up to 12 h. After that, the decrease in the surface treatment effect saturated and was maintained for up to 72 h (Figure S5). Though the unstable oxygen functional groups on the rCF surface decreased over time, the increase in surface roughness affected the increase in the dispersive component. The surface roughness of the rCFs increased as the voltage increased, and the curves occurred in the longitudinal direction of the rCFs (Figure S6). The increase in the surface roughness of the IPL-irradiated rCF was observed at the micrometer scale. The effective adhesion between the rCF and the polymer matrix is strongly dependent on the contact quality of the interface at the nanoscale and the associated chemical bonding strength (Jiang et al., 2014; Xie et al., 2011), which is dealt with in the next section.

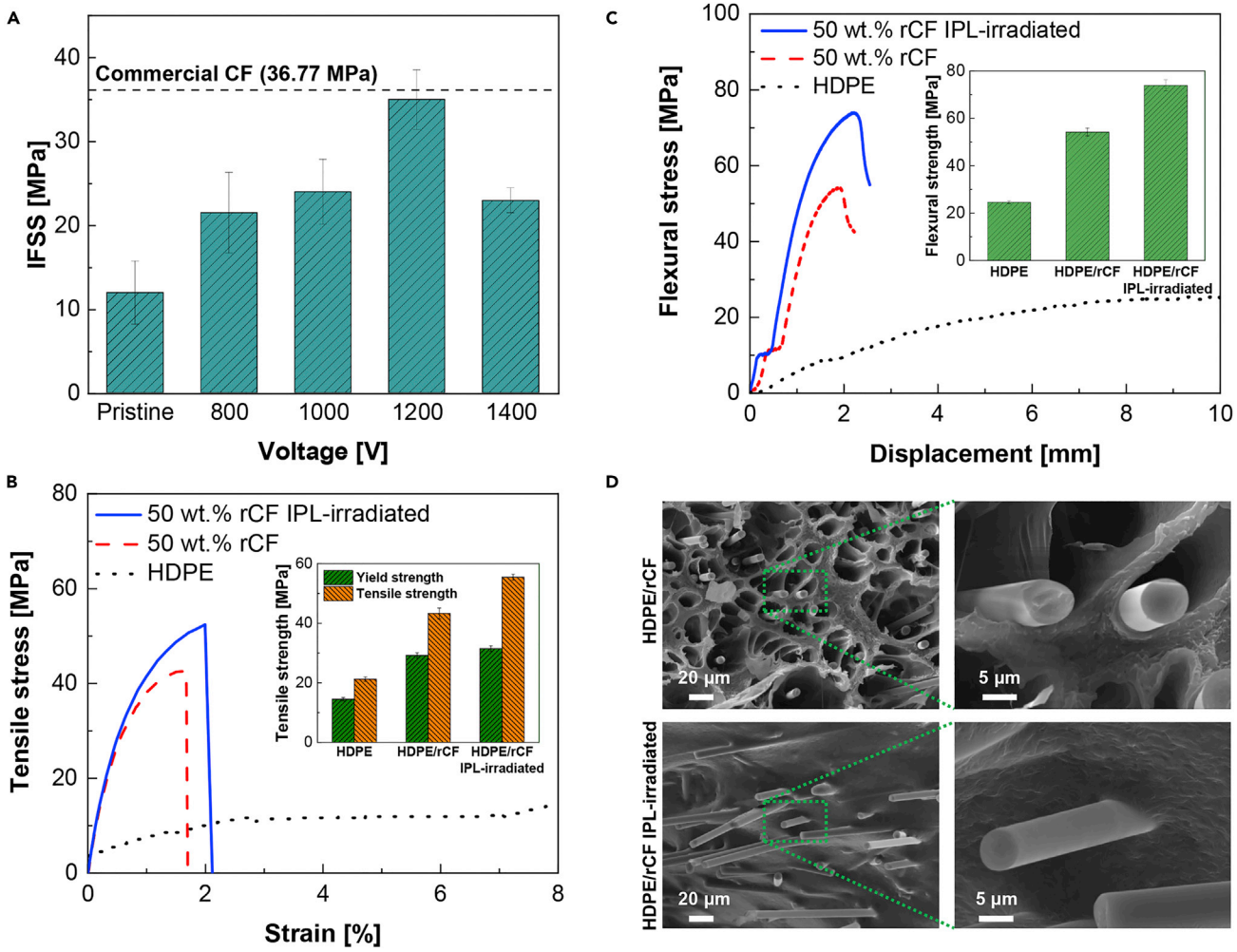

Figure 2. Controlling the interfacial bonding between rCF and HDPE by IPL irradiation and mechanical characteristics of HDPE/rCF composites

(A) IFSS of the rCFs IPL-irradiated at various voltages.

(B and C) Tensile stress-strain and flexural stress-displacement curves of HDPE and HDPE/rCFs composites.

(D) FE-SEM micrographs of the fracture surfaces of the HDEP/rCF composites.

Effects of IPL irradiation on IFSS of rCFs and mechanical properties of the HDPE/rCF composites

Interfacial shear strength (IFSS) measurement is an effective method for evaluating the interfacial adhesion between the CF and resin after surface treatment. The IFSS results for the pristine and IPL-irradiated rCFs are shown in Figure 2A. As the voltage was increased to 1,200 V, the IFSS increased from 11.9 to 35.0 MPa, which was 2.93 times higher than that of the pristine rCF, and 95% of that of the high-grade commercial CFs, Tansome H2550; the IFSS, then decreased to 22.95 MPa at 1,400 V, which was similar to the polar component of the surface energy (Figure 1B), and the O 1s/C 1s ratio (Table 1).

The tensile and flexural properties of the HDPE/rCF composites were evaluated, as shown in Figures 2B and 2C. The rCFs were IPL-irradiated at 1,200 V with 4 ms, 1 Hz, and 50 pulses, which was the condition for the highest IFSS; in addition, they were loaded to 50 wt % (Figure S7). After the IPL irradiation, the yield strength, tensile strength, and elongation increased. The tensile strength increased from 42.65 to 54.56 MPa, which was 27.3% higher than that before the IPL irradiation. The flexural properties exhibited a similar trend as that of the tensile properties. After the IPL irradiation, flexural strength and breaking distance increased; the flexural strength increased from 54.27 to 73.99 MPa, which was 36.3% higher than that before the IPL irradiation. The increase in the mechanical properties was considered to be owing to the combination of physical, chemical, and morphological changes of the surface after the IPL irradiation. The strengthening of the bonds between

carbon and oxygen after IPL irradiation enhanced the chemical interaction between the rCFs and HDPE matrix, facilitating a stress transfer in the HDPE/rCF composites. The roughened surface after the IPL irradiation increased the surface area of the rCF, which contributed to increasing the contact area with the matrix and strengthening the mechanical interlocking between the rCFs and HDPE matrix.

The fracture surfaces of the HDPE/rCF and HDPE/IPL-irradiated rCF composites are shown in Figure 2D. In the case of the HDPE/rCF composite, many holes were observed because of the fracture from the fibers pulling out of the matrix under loading. Holes were formed around the remaining rCFs, and most rCFs were debonded with the HDPE matrix. On the contrary, fracture surface of the HDPE/IPL-irradiated rCF composite exhibited rCFs fully bonded to the HDPE matrix. The fracture behavior conspicuously elucidated that the strong interfacial bonds were formed due to the high surface energy of the rCFs induced by IPL irradiation, resulting in the improved mechanical properties of the composite (Figures 2B and 2C).

Theoretical model of the formation of a strongly coupled interface in HDPE/rCF composites

All-atom MD simulations were performed to evaluate the possibility that C–O (and C=O) bonding of rCF formed during the IPL process enhances the interfacial bonding with HDPE. As oxygen coverage (OC) increased on the surface of graphite, the change in the non-covalent bond formed with HDPE was evaluated at the atomic level. In addition, the IFSS and stress distribution between the graphite and HDPE surfaces during the pull-out process of the graphite filler were calculated. Refer to Figures 3A and S8–S13 for the model preparation. The interfacial adhesion energy (E_{adh}) between the surfaces of the graphite oxide (GO) block and HDPE was calculated as follows:

$$E_{adh} = E_{sys} - E_{graphite} - E_{HDPE} \quad \text{(Equation 1)}$$

where E_{sys} is the potential energy of the bilayer system, and $E_{graphite}$ and E_{HDPE} are the potential energies of the isolated GO block and HDPE, respectively. The pull-out energy ($E_{adh}^{pullout}$) of the embedded GO block is defined as the difference in the interfacial adhesion energy between the initial state ($E_{adh}^{initial}$) and after the pull-out process ($E_{adh}^{current}$) and is calculated as follows (Yang et al., 2015; Gou et al., 2005):

$$E_{adh}^{pullout} = E_{adh}^{current} - E_{adh}^{initial} \quad \text{(Equation 2)}$$

$E_{adh}^{pullout}$ is the displacement-dependent cumulative quantity required to pull the embedded GO block out of the HDPE matrix. During the pull-out process, the IFSS of the HDPE/GO system was evaluated at the upper and lower interfaces with a constant width and linearly decreasing length according to the pull-out displacement. The total pull-out energy is expressed with respect to the displacement of the GO block in the x-direction:

$$E_{adh}^{pullout} = \int_0^{L_x} 2L_y(L_x - x)\tau dx \quad \text{(Equation 3)}$$

where τ is the magnitude of IFSS, and L_x and L_y are the cell dimensions in the x- and y-directions of the interface between the graphite and HDPE surfaces, respectively. The IFSS can be calculated by dividing the pull-out energy by the surface integral of the interfacial area bounded between HDPE and GO, as follows:

$$\tau = \frac{E_{adh}^{pullout}}{L_x^2 L_y} \quad \text{(Equation 4)}$$

In this regard, the pull-out energy and IFSS were calculated using Equations 3 and 4 during the time the GO block was in contact with HDPE. The average value of the calculated IFSS for each displacement step with different OCs is shown in Figure 3B. The IFSS significantly increased as the number density of the functional groups increased, which was strongly associated with the physical interlocking effects of surface roughness and non-bond interactions. Figure 3C shows the pull-out resistance of GO block. Figures 3D and S15 show the stress and displacement distributions of carbon atoms at the periphery of the functional groups. Accordingly, as depicted in Figure 3E, the honeycomb structure of the outermost GO layer became more distorted, as it moved away from the pulling position.

The results shown in Figure 3F clearly indicate that the compressive stress applied around the hydroxyl groups was higher than that around the epoxide groups, regardless of the OC (refer to supplemental information for the comparison according to the type of functional group). This is plausible from a structural point of view at a nanoscale. As the heights of the hydroxyl groups on the graphite surface were larger than

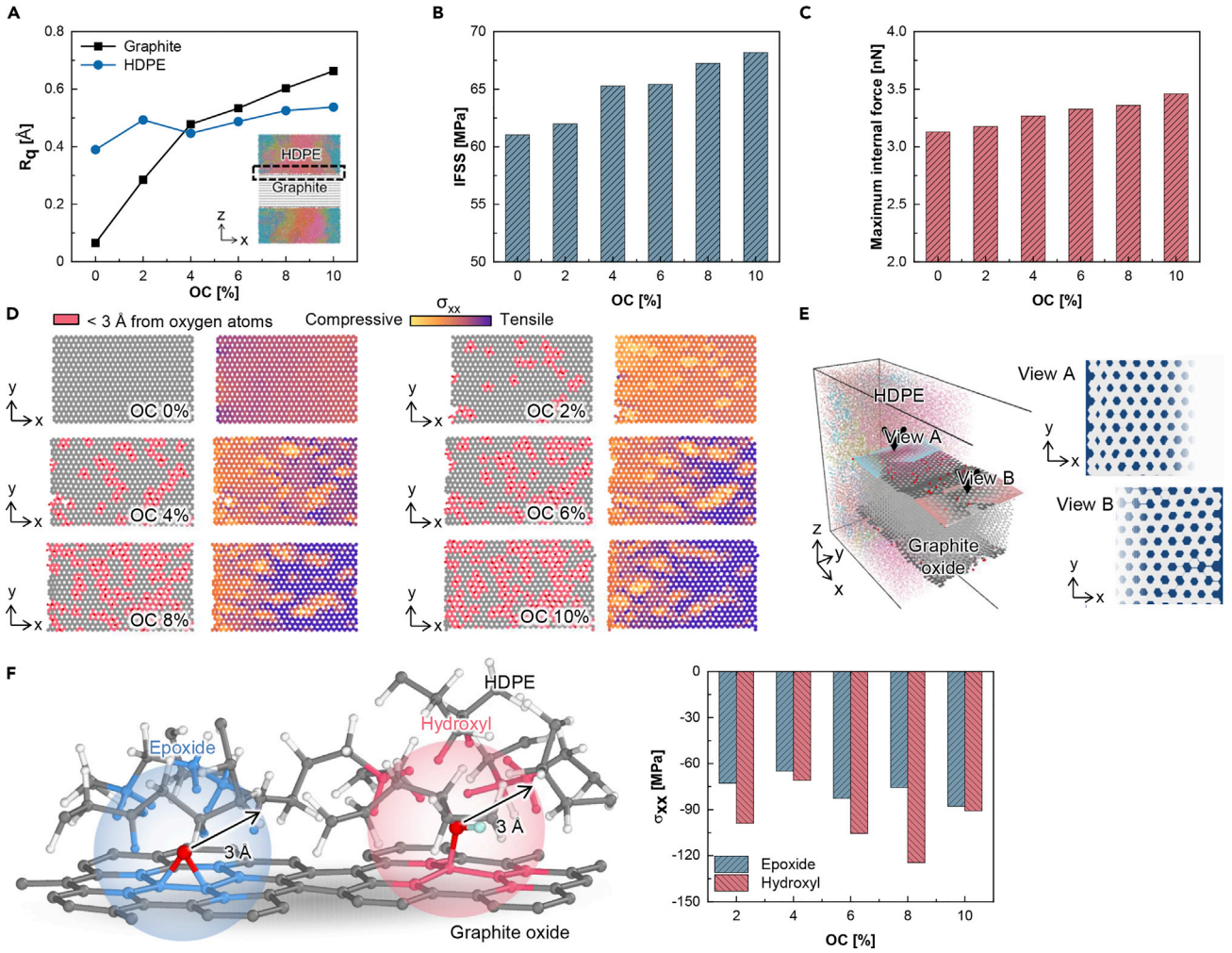

Figure 3. MD simulation results of the interfacial behaviors between the IPL-irradiated rCFs and HDPE matrix

(A) Estimated surface roughness of the upper interfaces between the GO block and HDPE with respect to OC.

(B) The IFSS values with different OC.

(C) Maximum internal force on the GO block during the pull-out process.

(D) From left to right, the GO surface (top surface of graphite) with the carbon atoms bonded to oxygen atoms are colored in pink, next to the GO surface of all carbon atoms are colored according to color scale of atomic stress in the x-direction. The carbon atoms bonded to the functional oxygen groups at a pull-out displacement of 20 Å.

(E) GO block of 6% OC inside the HDPE matrix at a pull-out displacement of 30 Å and detailed cross-sectional views of the GO surface; the voids between the bright carbon atoms are in a dark shade.

(F) Spherical regions in the vicinity of epoxide and hydroxyl groups and the corresponding compressive stresses in the x-direction during the pull-out test.

those of the epoxide groups, the effective surface area that could form non-bonded interactions with the HDPE surface increased as well.

The present MD simulations describe the molecular-scale mechanical interlocking effect from the materials and structural perspectives. Evidently, the IPL process still cannot rule out the possibility of other physico-chemical factors, such as the breaking of the generated bonds and the formation of other chemically bonding species that contribute to interfacial bonding. Nevertheless, the IFSS values predicted by the MD simulations were comparable to experimental values. Furthermore, the XPS intensity data in Figures 1C–1E indicated that the concentration of the O–C bonds on the rCF surface, corresponding to the strongest "oxygen - carbon" non-bonded interactions, allowed for presumed IFSS variations. Therefore, the molecular-scale interaction characteristics of the GO group and HDPE can be understood as it is the dominant factor explaining the effect of the IPL process.

DISCUSSION

A process technology that reuses waste resources and treats them close to off-the-shelf performance is clearly attractive. Important points to consider in this process are that the time required for reprocessing is fast enough, the cost is low due to the simple procedure, and the principle of the improvement effect must be clearly supported. In this study, by applying the IPL process to waste carbon fibers, we succeeded in obtaining a result that satisfies all of the above requirements. After IPL irradiation, the rCF surface was functionalized with C–O and C=O bonds and roughened with curves and grooves to improve adhesion between HDPEs. To precisely identify the conditions for maximizing the surface modification characteristics, the irradiation voltage was sequentially changed from 800 to 1,400 V. As a result, it was confirmed that the surface energy of rCF can attain a maximum of 50.3 mN/m at 1,200 V. The IFSS of the IPL-irradiated rCFs also showed a similar trend, with a maximum of 35.0 MPa at 1,200 V, which was 95% of that of commercial CF. The tensile and flexural strengths of the HDPE/rCF composites were practically increased by 1.27 and 1.36 times, respectively, compared to those of the pristine composite.

Meanwhile, the XPS analysis results showed that the increased composition ratios of C–O and C=O bonds after IPL irradiation were highly correlated with the improvement in interfacial bonding strength. The generated chemical bonds were the result of partial oxidation of the surface of rCF by IPL irradiation. Thus, it is necessary to understand how they contribute to the improvement of the interfacial bonding strength of the composite materials from a physicochemical viewpoint. In this regard, the surface oxidation effect of rCF on the IFSS of rCF/HDPE was further theoretically investigated using MD simulations. The MD simulation results show that the IFSS of the system increases by approximately 1.11 times as the OC increases within the considered conditions. This increase was the result of the oxide groups forming energy pairs having strong, non-covalent interaction and adjacent HDPE constituent atoms. In addition, the oxygen groups on the graphite surface led to structural distortion and local stress concentration, resulting in an increase in the interfacial adhesion between the rCFs and HDPE matrix. As the surface roughness of the outermost graphite was used to determine the approximate intrinsic surface roughness of the adjacent HDPE, molecular-scale interlocking was achieved, enabling effective load transfer. In summary, the MD simulation results indicate that the generation of the oxidized groups by IPL irradiation enhances their chemical interaction with HDPE and assists in molecular interlocking at the interface. These findings can be further applied to optimize the IPL irradiation process, which is strongly desired for practical applications of rCF-based composites.

Limitations of the study

This work is the first empirical study on a process that can actually increase the usability of recycled carbon fiber, and thus the following open questions remain. First, the experiments provided quantitative values for adsorption and physical interlocking at the interface with HDPE, but the used HDPE was well refined and not a recycled material. The amount of change in IFSS by the output voltage of the Xenon lamp was found to be significant, suggesting that the optimization of the interface performance is still required in the future. The interfacial bonding force and load transfer characteristics identified in the MD simulation were limitedly investigated only for two representative oxidation reactions (epoxy and hydroxyl groups) that can occur on the graphite surface. The productivity evaluation of practical engineering applications through the enlargement and mass production of waste resource recycling is still outside the scope of this study. Efforts to address the above challenges are all necessary to bring the findings of this study into a practical engineering field.

STAR★METHODS

Detailed methods are provided in the online version of this paper and include the following:

- KEY RESOURCES TABLE
- RESOURCE AVAILABILITY
  - Lead contact
  - Materials availability
  - Data and code availability
- METHOD DETAILS
  - Materials
  - IPL treatment of rCF
  - Preparation of HDPE/rCF composites

- Characterization and measurements
- Molecular dynamics (MD) simulations

SUPPLEMENTAL INFORMATION

Supplemental information can be found online at https://doi.org/10.1016/j.isci.2022.105367.

ACKNOWLEDGMENTS

This study was conducted with the support of Korea Institute of Industrial Technology under the programs (KITECH JB-21-0010, KITECH JD-22-0009)" and Basic Science Research Program through the National Research Foundation of Korea (NRF), funded by the Ministry of Education (No. 2022R1F1A1063199). This study was also partly supported by a grant (RA202004-5-C4) from Jeonbuk Research and Development Program funded by Jeonbuk Province. Also, this work was supported by the Ministry of Trade, Industry and Energy (MOTIE) (grant 20016789).

AUTHOR CONTRIBUTIONS

Under supervision by K.-S.K. and J.C., M.K. performed experiment design, data analysis and paper written, and B.G. performed computational simulation and paper written. J.K. developed sample preparation and analysis. All authors read and contributed to the manuscript.

DECLARATION OF INTERESTS

The authors declare that they have no known competing financial interests or personal relationships that could have appeared to influence the work reported in this paper.

Received: June 30, 2022
Revised: September 12, 2022
Accepted: October 12, 2022
Published: November 18, 2022

REFERENCES

Al-Hamry, A., Kang, H., Sowade, E., Dzhagan, V., Rodriguez, R.D., Müller, C., Zahn, D.R.T., Baumann, R.R., and Kanoun, O. (2016). Tuning the reduction and conductivity of solution-processed graphene oxide by intense pulsed light. Carbon *102*, 236–244. https://doi.org/10.1016/j.carbon.2016.02.045.

Andersen, H.C. (1980). Molecular dynamics simulations at constant pressure and/or temperature. J. Chem. Phys. *72*, 2384–2393. https://doi.org/10.1063/1.439486.

Babilas, P., Schreml, S., Szeimies, R.M., and Landthaler, M. (2010). Intense pulsed light (IPL): a review. Lasers Surg. Med. *42*, 93–104. https://doi.org/10.1002/lsm.20877.

Bitter, P.H. (2000). Noninvasive rejuvenation of photodamaged skin using serial, full-face intense pulsed light treatments. Dermatol. Surg. *26*, 835–842. , discussion: 843. https://doi.org/10.1046/j.1524-4725.2000.00085.x.

Berendsen, H.J.C., Postma, J.P.M., van Gunsteren, W.F., DiNola, A., and Haak, J.R. (1984). Molecular dynamics with coupling to an external bath. J. Chem. Phys. *81*, 3684–3690. https://doi.org/10.1063/1.448118.

Błażejewski, W., Filipiak, A., Barcikowski, M., Łagoda, K., Stabla, P., Lubecki, M., Stosiak, M., Śliwiński, C., and Kamyk, Z. (2018). Design and implementing possibilities of composite pontoon bridge. Zesz. Nauk. Politech. Rzeszowskiej. Mech. *35*, 411–420. https://doi.org/10.7862/rm.2018.35.

Boukhvalov, D.W. (2014). Oxidation of a graphite surface: the role of water. J. Phys. Chem. C *118*, 27594–27598. https://doi.org/10.1021/jp509659p.

Boukhvalov, D.W., Katsnelson, M.I., and Lichtenstein, A.I. (2008). Hydrogen on graphene: electronic structure, total energy, structural distortions and magnetism from first-principles calculations. Phys. Rev. B *77*, 035427. https://doi.org/10.1103/PhysRevB.77.035427.

Brewis, D.M., and Briggs, D. (1981). Adhesion to polyethylene and polypropylene. Polymer *22*, 7–16. https://doi.org/10.1016/0032-3861(81)90068-9.

Cai, G., Wada, M., Ohsawa, I., Kitaoka, S., and Takahashi, J. (2019). Interfacial adhesion of recycled carbon fibers to polypropylene resin: effect of superheated steam on the surface chemical state of carbon fiber. Compos. Appl. Sci. Manuf. *120*, 33–40. https://doi.org/10.1016/j.compositesa.2019.02.020.

Caltagirone, P.E., Ginder, R.S., Ozcan, S., Li, K., Gay, A.M., Stonecash, J., Steirer, K.X., Cousins, D., Kline, S.P., Maxey, A.T., and Stebner, A.P. (2021). Substitution of virgin carbon fiber with low-cost recycled fiber in automotive grade injection molding polyamide 66 for equivalent composite mechanical performance with improved sustainability. Compos. B Eng. *221*, 109007. https://doi.org/10.1016/j.compositesb.2021.109007.

Cassagneau, T., Guérin, F., and Fendler, J.H. (2000). Preparation and characterization of ultrathin films layer-by-layer self-assembled from graphite oxide nanoplatelets and polymers. Langmuir *16*, 7318–7324. https://doi.org/10.1021/la000442o.

Chen, S.J., Li, C.Y., Wang, Q., and Duan, W.H. (2017). Reinforcing mechanism of graphene at atomic level: friction, crack surface adhesion, and 2D geometry. Carbon *114*, 557–565. https://doi.org/10.1016/j.carbon.2016.12.034.

Chukov, D.I., Stepashkin, A.A., Maksimkin, A.V., Tcherdyntsev, V.V., Kaloshkin, S.D., Kuskov, K.V., and Bugakov, V.I. (2015). Investigation of structure, mechanical and tribological properties of short carbon fiber reinforced UHMWPE-matrix composites. Compos. B Eng. *76*, 79–88. https://doi.org/10.1016/j.compositesb.2015.02.019.

Dai, Z., Zhang, B., Shi, F., Li, M., Zhang, Z., and Gu, Y. (2011). Effect of heat treatment on carbon fiber surface properties and fibers/epoxy interfacial adhesion. Appl. Surf. Sci. *257*, 8457–8461. https://doi.org/10.1016/j.apsusc.2011.04.129.

Elias, D.C., Nair, R.R., Mohiuddin, T.M.G., Morozov, S.V., Blake, P., Halsall, M.P., Ferrari, A.C., Boukhvalov, D.W., Katsnelson, M.I., Geim, A.K., and Novoselov, K.S. (2009). Control of graphene's properties by reversible hydrogenation: evidence for graphene. Science *323*, 610–613. https://10.1126/science.1167130.

Fan, Z.J., Williams, M.C., and Choi, P. (2002). A molecular dynamics study of the effects of branching characteristics of LDPE on its miscibility with HDPE. Polymer *43*, 1497–1502. https://doi.org/10.1016/S0032-3861(01)00730-3.

Fonseca, A.F., Zhang, H., and Cho, K. (2015). Formation energy of graphene oxide structures: a molecular dynamics study on distortion and thermal effects. Carbon *84*, 365–374. https://doi.org/10.1016/j.carbon.2014.12.026.

Gao, Y., Liu, L.Q., Zu, S.Z., Peng, K., Zhou, D., Han, B.H., and Zhang, Z. (2011). The Effect of interlayer adhesion on the mechanical behaviors of macroscopic graphene oxide papers. ACS Nano *5*, 2134–2141. https://doi.org/10.1021/nn103331x.

Ghaderi, N., and Peressi, M. (2010). First-principle study of hydroxyl functional groups on pristine, defective graphene, and graphene epoxide. J. Phys. Chem. C *114*, 21625–21630. https://doi.org/10.1021/jp108688m.

Gou, J., Liang, Z., Zhang, C., and Wang, B. (2005). Computational analysis of effect of single-walled carbon nanotube rope on molecular interaction and load transfer of nanocomposites. Compos. B Eng. *36*, 524–533. https://doi.org/10.1016/j.compositesb.2005.02.004.

He, H., Klinowski, J., Forster, M., and Lerf, A. (1992). A new structural model for graphite oxide. Chem. Phys. Lett. *287*, 53–56. https://doi.org/10.1016/S0009-2614(98)00144-4.

Hestenes, M.R., and Stiefel, E. (1952). Method of conjugate gradients for solving linear systems. J. Res. Natl. Bur. Stand. *49*, 409–435. https://cir.nii.ac.jp/crid/1571135650579367168.

Heyes, D.M. (1994). Pressure tensor of partial-charge and point-dipole lattices with bulk and surface geometries. Phys. Rev. B Condens. Matter *49*, 755–764. https://doi.org/10.1103/PhysRevB.49.755.

Holmes, M. (2018). Recycled carbon fiber composites become a reality. Reinforc. Plast *62*, 148–153. https://doi.org/10.1016/j.repl.2017.11.012.

Hontoria-Lucas, C., López-Peinado, A., López-González, J.D., Rojas-Cervantes, M.L., and Martín-Aranda, R. (1995). Study of oxygen-containing groups in a series of graphite oxides: physical and chemical characterization. Carbon *33*, 1585–1592. https://doi.org/10.1016/0008-6223(95)00120-3.

Jacob, A. (2014). Carbon fibre and cars – 2013 in review. Reinforc. Plast *58*, 18–19. https://doi.org/10.1016/S0034-3617(14)70036-0.

Jang, B.Z. (1992). Control of interfacial adhesion in continuous carbon and Kevlar fiber-reinforced polymer composites. Compos. Sci. Technol. *44*, 333–349. https://doi.org/10.1016/0266-3538(92)90070-J.

Jang, J., and Yang, H. (2000). The effect of surface treatment on the performance improvement of carbon fiber/polybenzoxazine composites. J. Mater. Sci. *35*, 2297–2303. https://doi.org/10.1023/A:1004791313979.

Jiang, D., Xing, L., Liu, L., Yan, X., Guo, J., Zhang, X., Zhang, Q., Wu, Z., Zhao, F., Huang, Y., et al. (2014). Interfacially reinforced unsaturated polyester composites by chemically grafting different functional POSS onto carbon fibers. J. Mater. Chem. *2*, 18293–18303. https://doi.org/10.1039/C4TA04055D.

Jiu, J., Nogi, M., Sugahara, T., Tokuno, T., Araki, T., Komoda, N., Suganuma, K., Uchida, H., and Shinozaki, K. (2012). Strongly adhesive and flexible transparent silver nanowire conductive films fabricated with a high-intensity pulsed light technique. J. Mater. Chem. *22*, 23561–23567. https://doi.org/10.1039/C2JM35545K.

Kim, B.H., Lee, D.H., Yang, K.S., Lee, B.C., Kim, Y.A., and Endo, M. (2011). Electron beam irradiation-enhanced wettability of carbon fibers. ACS Appl. Mater. Interfaces *3*, 119–123. https://doi.org/10.1021/am101064s.

Kang, J.S., Ryu, J., Kim, H.S., and Hahn, H.T. (2011). Sintering of inkjet-printed silver nanoparticles at room temperature using intense pulsed light. J. Electron. Mater. *40*, 2268–2277. https://doi.org/10.1007/s11664-011-1711-0.

Kim, H.S., Djage, S.R., and Shim, D.E. (2009). Intense plused light sintering of copper nanoink for printed electronics. Appl. Phys. A *97*, 791–798. https://doi.org/10.1007/s00339-009-5360-6.

Kim, J.-H., Lee, C.-J., Min, K.D., Hwang, B.-U., Kang, D.G., Choi, D.H., Joo, J., and Jung, S.-B. (2021). Intense pulsed light surface treatment for improving adhesive bonding of aluminum and carbon fiber-reinforced plastic (CFRP). Compos. Struct. *258*, 113364. https://doi.org/10.1016/j.compstruct.2020.113364.

Kouparitsas, C.E., Kartalis, C.N., Varelidis, P.C., Tsenoglou, C.J., and Papaspyrides, C.D. (2002). Recycling of the fibrous fraction of reinforced thermoset composites. Polym. Compos. *23*, 682–689. https://doi.org/10.1002/pc.10468.

Lahaye, R.J.W.E., Jeong, H.K., Park, C.Y., and Lee, Y.H. (2009). Density functional theory study of graphite oxide for different oxidation levels. Phys. Rev. B *79*, 125435. https://doi.org/10.1103/PhysRevB.79.125435.

Lee, S., Park, S.H., Jang, K., Yu, S., Song, C., Kim, H.S., and Ahn, H. (2017). Simple, ultra-rapid, versatile method to synthesize cobalt/cobalt oxide nanostructures on carbon fiber paper via intense pulsed white light (IPWL) photothermal reduction for energy storage applications. J. Alloys Compd. *724*, 684–694. https://doi.org/10.1016/j.jallcom.2017.07.069.

Lee, S.M., Lee, Y.H., Hwang, Y.G., Hahn, J.R., and Kang, H. (1999). Defect-induced oxidation of graphite. Phys. Rev. Lett. *82*, 217–220. https://doi.org/10.1103/PhysRevLett.82.217.

Lerf, A., He, H., Riedl, T., Forster, M., and Klinowski, J. (1997). 13C and 1H MAS NMR studies of graphite oxide and its chemically modified derivatives. Solid State Ion. *101–103*, 857–862. https://doi.org/10.1016/S0167-2738(97)00319-6.

Lim, J., Goh, B., Qu, W., Kim, Y., Choi, J., and Hong, S. (2022). Adhesive-free bonding of PI/PDMS interface by site-selective photothermal reactions. Appl. Surf. Sci. *571*, 151123. https://doi.org/10.1016/j.apsusc.2021.151123.

Liu, X., Li, X., Liu, J., Wang, Z., Kong, B., Gong, X., Yang, X., Lin, W., and Guo, L. (2014). Study of high-density polyethylene (HDPE) pyrolysis with reactive molecular dynamics. Polym. Degrad. Stab. *104*, 62–70. https://doi.org/10.1016/j.polymdegradstab.2014.03.022.

McNally, T., Boyd, P., McClory, C., Bien, D., Moore, I., Millar, B., Davidson, J., and Carroll, T. (2008). Recycled carbon fiber-filled polyethylene composites. J. Appl. Polym. Sci. *107*, 2015–2021. https://doi.org/10.1002/app.27253.

Meng, F., McKechnie, J., Turner, T., Wong, K.H., and Pickering, S.J. (2017). Environmental aspects of use of recycled carbon fiber composites in automotive applications. Environ. Sci. Technol. *51*, 12727–12736. https://doi.org/10.1016/j.compositesb.2021.109007.

Olgun, U., and Kalyon, D.M. (2005). Use of molecular dynamics to investigate polymer melt–metal wall interactions. Polymer *46*, 9423–9433. https://doi.org/10.1016/j.polymer.2005.07.042.

Osbeck, S., Bradley, R.H., Liu, C., Idriss, H., and Ward, S. (2011). Effect of an ultraviolet/ozone treatment on the surface texture and functional groups on polyacrylonitrile carbon fibers. Carbon *49*, 4322–4330. https://doi.org/10.1016/j.carbon.2011.06.005.

Pei, L., and Li, Y.F. (2017). Rapid and efficient intense pulsed light reduction of graphene oxide inks for flexible printed electronics. RSC Adv. *7*, 51711–51720. https://doi.org/10.1039/C7RA10416B.

Pittman, C., He, G.R., Wu, B., and Gardner, S.D. (1997). Chemical modification of carbon fiber surfaces by nitric acid oxidation followed by reaction with tetraethylenepentamine. Carbon *35*, 317–331. https://doi.org/10.1016/S0008-6223(97)89608-X.

Plimpton, S. (1995). Fast parallel algorithms for short-range molecular dynamics. J. Comput. Phys. *117*, 1–19. https://doi.org/10.1006/jcph.1995.1039.

Rich, M.J., Drown, E.K., Askeland, P., and Drzal, L.T. (2013). Surface treatment of carbon fibers by ultraviolet light+ ozone: its effect on fiber surface area and topography. In Proceedings of the ICCM Conference, Suong Van Hoa and Pascal Hubert, eds. (International Committee on Composite Materials), pp. 1196–1204.

Servinis, L., Beggs, K.M., Gengenbach, T.R., Doeven, E.H., Francis, P.S., Fox, B.L., Pringle, J.M., Pozo-Gonzalo, C., Walsh, T.R., and Henderson, L.C. (2017). Tailoring the fiber-to-matrix interface using click chemistry on carbon fiber surfaces. J. Mater. Chem. *5*, 11204–11213. https://doi.org/10.1039/C7TA00922D.

Shin, H., Kim, K.K., Benayad, A., Yoon, S., Park, H.K., Jung, I., Jin, M.H., Jeong, H., Kim, J.M., Choi, J., and Lee, Y.H. (2009). Efficient reduction of graphite oxide by sodium borohydride and its effect on electrical conductance. Adv. Funct. Mater. *19*, 1987–1992. https://doi.org/10.1002/adfm.200900167.

Soutis, C. (2005). Fiber reinforced composites in aircraft construction. Prog. Aero. Sci. *41*, 143–151. https://doi.org/10.1016/j.paerosci.2005.02.004.

Sun, H., Mumby, S.J., Maple, J.R., and Hagler, A.T. (1994). An ab initio CFF93 all-atom force field for polycarbonates. J. Am. Chem. Soc. *116*, 2978–2987. https://doi.org/10.1021/ja00086a030.

Vinod, S., Tiwary, C.S., Samanta, A., Ozden, S., Narayanan, T.N., Vajtai, R., Agarwal, V., Singh, A.K., John, G., and Ajayan, P.M. (2018). Graphene oxide epoxy (GO-xy): GO as epoxy adhesive by interfacial reaction of functionalities. Adv. Mater. Interfaces *5*, 1700657. https://doi.org/10.1002/admi.201700657.

Wang, Y., Zhang, S., Luo, D., and Shi, X. (2019). Effect of chemically modified recycled carbon fiber composite on the mechanical properties of cementitious mortar. Compos. B Eng. *173*, 106853. https://doi.org/10.1016/j.compositesb.2019.05.064.

Wernik, J.M., Cornwell-Mott, B.J., and Meguid, S.A. (2012). Determination of the interfacial properties of carbon nanotube reinforced polymer composites using atomistic-based continuum model. Int. J. Solids Struct. *49*, 1852–1863. https://doi.org/10.1016/j.ijsolstr.2012.03.024.

Xie, J., Xin, D., Cao, H., Wang, C., Zhao, Y., Yao, L., Ji, F., and Qiu, Y. (2011). Improving carbon fiber adhesion to polyimide with atmospheric pressure plasma treatment. Surf. Coat. Technol. *206*, 191–201. https://doi.org/10.1016/j.surfcoat.2011.04.016.

Xiong, C., Li, Q., Lan, T., Li, H., Long, W., and Xing, F. (2021). Sustainable use of recycled carbon fiber reinforced polymer and crumb rubber in concrete: mechanical properties and ecological evaluation. J. Clean. Prod. *279*, 123624. https://doi.org/10.1016/j.jclepro.2020.123624.

Yan, J.A., and Chou, M.Y. (2010). Oxidation functional groups on graphene: structural and electronic properties. Phys. Rev. B *82*, 125403. https://doi.org/10.1103/PhysRevB.82.125403.

Yang, S., Choi, J., and Cho, M. (2015). Intrinsic defect-induced tailoring of interfacial shear strength in CNT/polymer nanocomposites. Compos. Struct. *127*, 108–119. https://doi.org/10.1016/j.compstruct.2015.02.078.

Yang, S., Shin, H., and Cho, M. (2021). Contribution of oxygen functional groups in graphene to the mechanical and interfacial behavior of nanocomposites: molecular dynamics and micromechanics study. Int. J. Mech. Sci. *189*, 105972. https://doi.org/10.1016/j.ijmecsci.2020.105972.

Yao, S.S., Jin, F.L., Rhee, K.Y., Hui, D., and Park, S.J. (2018). Recent advances in carbon fiber-reinforced thermoplastic composites: a review. Compos. B Eng. *142*, 241–250. https://doi.org/10.1016/j.compositesb.2017.12.007.

Youn, J.W., Lee, S.J., Kim, K.-S., and Kim, D.U. (2018). Adhesion characteristics of VO_2 ink film sintered by intense pulsed light for smart window. Appl. Surf. Sci. *441*, 508–514. https://doi.org/10.1016/j.apsusc.2018.02.061.

Yu, H., Liu, G., Wang, M., Ren, R., Shim, G., Kim, J.Y., Tran, M.X., Byun, D., and Lee, J.K. (2020). Plasma-assisted surface modification on the electrode interface for flexible fiber-shaped Zn–polyaniline batteries. ACS Appl. Mater. Interfaces *12*, 5820–5830. https://doi.org/10.1016/j.surfcoat.2011.04.016.

Zhang, G., Sun, S., Yang, D., Dodelet, J.P., and Sacher, E. (2008). The surface analytical characterization of carbon fibers functionalized by H_2SO_4/HNO_3 treatment. Carbon *46*, 196–205. https://doi.org/10.1016/j.carbon.2007.11.002.

Zhao, S., Zhang, Y., Yang, J., and Kitipornchai, S. (2021). Significantly improved interfacial shear strength in graphene/copper nanocomposite via wrinkles and functionalization: a molecular dynamics study. Carbon *174*, 335–344. https://doi.org/10.1016/j.carbon.2020.12.026.

STAR★METHODS

KEY RESOURCES TABLE

REAGENT or RESOURCE	SOURCE	IDENTIFIER
Chemicals, peptides, and recombinant proteins		
Acetone	Daejung Chemicals & Metals Co., Ltd., South Korea	CAS: 67-64-1
UHP Ar, 99.999%	Milsung Industrial Gas Co., Ltd., South Korea	CAS: 7440-37-1
UHP Oxygen, 99.999%	Milsung Industrial Gas Co., Ltd., South Korea	CAS: 7782-44-7
HDPE	Lotte Chemical Co., Ltd., South Korea	HDPE 2200J
Distilled water	Daejung Chemicals & Metals Co., Ltd., South Korea	CAS: 7732-18-5
Diiodomethane	Sigma-Aldrich Co., Ltd., USA	CAS: 75-11-6
Software and algorithms		
XPSPEAK 4.1	Raymund W.M. Kwok, The Chinese University of Hong Kong	https://xpspeak.software.informer.com/4.1/
BIOVIA Materials Studio 5.5	Dassault Systèmes Biovia Co., Ltd., France	https://accelrys-materials-studio.software.informer.com/5.5/
LAMMPS 64-bit 18Jun2019	Sandia National Laboratories	https://github.com/lammps/lammps
Other		
rCFs	Hyosung Advanced Materials Co., Ltd., South Korea	N/A
T700 CFs	Hyosung Advanced Materials Co., Ltd., South Korea	Tansome® H2550

RESOURCE AVAILABILITY

Lead contact

Further information and requests for resources and reagents should be directed to and will be fulfilled by the Lead Contact, Kwang-Seok Kim (ore21@kitech.re.kr).

Materials availability

This study did not generate new unique reagents.

Data and code availability

This study did not generate/analyze data sets/code. All data are described in the main text and methods.

METHOD DETAILS

Materials

The rCFs were procured from Hyosung, Korea. The rCFs had a linear density of 0.60 denier and a tensile strength of 3.92 GPa. HDPE pellets were purchased from Lotte Chemical, Korea (2200 J). The pellets had a density of 0.965 g/cm^3 and a melt flow rate of 5.0 g/10 min.

IPL treatment of rCF

An IPL system (HI-PULSE, PSTEK, Korea) consists of a xenon flash lamp, lamp house, power supply, and water cooler. The main parameters of the IPL treatment are the voltage, pulse width, frequency, and number of pulses. In the present study, the voltage was varied from 800 to 1,400 V in steps of 200 V under fixed

conditions of 4 ms, 1 Hz, and 50 pulses. Argon and oxygen gas were passed through the chamber at a rate of 198 and 2 sccm, respectively, at a working pressure of 1.5×10^{1} Torr.

Preparation of HDPE/rCF composites

Each rCF, with or without the IPL treatment was physically mixed with the HDPE pellets, and each mixture containing 50 wt.% of rCF was discharged into a twin-screw extruder (STS25, Hankook E.M. Ltd, Korea). The extrusion temperature and screw speed were 230°C and 30 rpm, respectively. The extruded materials were collected and chopped to form pellets. The pelletized composites were placed into an injection machine (PF120, Dongshin Hydraulics, Korea), and then injected into the mold with five temperature zones. The temperature profiles of the five zones were: 200 (die zone), 210, 200, 190, and 180°C. The HDPE/rCF composites were molded for tensile and flexural tests according to ASTM D 638 and ASTM D 790M standards, respectively.

Characterization and measurements

Surface energy measurement

The surface energy of the CFs was measured according to the Wilhelmy method using a surface tensiometer for a single filament (K100SF, Krüss, Germany). Forces during the insertion and extraction of a single fiber through the testing liquids were detected using a microbalance. With this force, the dynamic contact angles at advancing and receding velocities can be calculated as follows:

$$F_{measured} = F_{fiber} + F_{wetting} - F_{buoyancy} \quad \text{(Equation 5)}$$

where $F_{measured}$ is the force detected by the microbalance; F_{fiber} is the gravitation of the fiber; and $F_{buoyancy}$ is the buoyancy force of the fiber in the testing liquid. In this study, $F_{buoyancy}$ was neglected, as it was insignificant compared to the capillary force of CF. F_{fiber} was set to zero at the start of each experimental run and the equation for the calculation is as follows:

$$F_{measured} = F_{fiber} = \gamma \cdot P \cdot \cos\theta \quad \text{(Equation 6)}$$

where P is the perimeter of the CF; θ is the dynamic contact angle; and γ is the surface tension of the testing liquid. The surface energy of a CF is the sum of the polar and dispersive components, which are calculated using the Owens-Wendt equation as follows:

$$W_a = \gamma_L(1 + \cos\theta) = 2\left(\gamma_s^p \gamma_L^p\right)^{\frac{1}{2}} + 2\left(\gamma_s^d \gamma_L^d\right)^{\frac{1}{2}} \quad \text{(Equation 7)}$$

where γ_L is the liquid surface free energy, γ_S is the solid surface energy, and p and d the polar and dispersive components, respectively. Here, γ_L, γ_L^p, γ_L^d are known values; and γ_s^p and γ_s^d can be calculated from the measured contact angle. Distilled water and diiodomethane were used as the testing liquids in this study. The measurements were conducted at a detection speed of 9 mm/min and a measuring speed of 4.5 mm/min, and with a detection threshold of 1×10^{-6} g and an immersion depth of 5 mm.

Surface chemical characteristics

The surface chemical compositions and bonds were analyzed using an X-ray photoelectron spectrometer (Thermo/K-Alpha ESCA System, Thermo Fisher Scientific, USA) with an Al Kα source in a vacuum chamber at 5×10^{-9} Mbar. CF bundles on copper tape were exposed to the X-ray beam, and data processing was conducted using the XPSPEAK 4.1 software. The C 1s peaks of all the samples were normalized and deconvoluted to C–C, C=C, C–O, and C=O functions using the Lorentzian–Gaussian function.

Surface roughness and topography analysis

The surface topologies of pristine and IPL-treated rCFs were analyzed using high-resolution atomic force microscopy (HR-AFM) (NX10, Park Systems, Korea). A $2 \times 2\ \mu m^2$ area of each sample was measured and the changes in the nanoscale roughness at various voltages were compared.

Determination of interfacial shear strength (IFSS)

The IFSS of the CFs was investigated using a micro-droplet test. Tansome® H2550 (Hyosung, Korea) was used as a commercial CF, and the IFSS value was an experimental value measured in the same manner as that of the rCF. A resin was dropped onto a single CF and cured for 72 h at room temperature. After fixing a single strand of the CF to a paper frame, HDPE was melted onto a single rCF. The size of the micro-droplet fixed between two blades was measured using an optical micrometer. Tensile tests were performed at a

rate of 0.03 mm/min until the micro-droplets ruptured, at which time the IFSS between the rCF and HDPE was calculated using the following equation:

$$\tau_{max} = \frac{F_d}{\pi D_f L_e} \quad \text{(Equation 8)}$$

where τ_{max} is the IFSS; F_d is the maximum load; D_f is the rCF diameter; and L_e is the embedded length. Equation 8 assumes a uniform shear lag model of the cylindrical single rCF with the surrounding resin, where the shear stresses are uniformly distributed along the rCF–resin interface.

Mechanical properties of the HDPE/rCF composites

Tensile and three-point bending flexural tests were performed using a universal testing machine (Instron5982, Instron, USA) to determine the tensile and flexural strengths of the HDPE/rCF composites subject to IPL irradiation. These two types of tests were conducted at equivalent speeds of 5 and 2 mm/min, respectively. Fifteen specimens were tested for each condition, and the averages of the fifteen values measured were included in the data presented.

Microstructure observation

After tensile tests, fracture segments were mounted on the standard holder using carbon adhesive, and coated with platinum in the sputter coater (Cressington, Cressington 108 Auto, UK). The morphology and structure of the fracture surface were characterized by a field emission scanning electron microscopy (FE-ESM, JSM-7100F, JEOL, Japan).

Molecular dynamics (MD) simulations

Unit cell modeling

MD simulations were performed to quantify the surface modification characteristics of the oxygen functional groups on the rCF surface. A set of 17 molecular structures of the HDPE chains consisting of 500 repeat monomer units was prepared to construct a periodic amorphous cell model, as shown in Figure S8A. The HDPE chains were distributed inside a cuboid-shaped box of dimensions of 5.00, 9.95, and 8.21 nm in the x-, y-, and z-directions, respectively (see Figure S8B). The target density of the HDPE amorphous cell was set to 0.97 g/cm^3 (Liu et al., 2014; Olgun and Kalyon, 2005; Fan et al., 2002). The potential energy of the amorphous HDPE was minimized using the conjugate gradient method (Hestenes and Stiefel, 1952). The thermally relaxed configuration of the amorphous HDPE was obtained at 300 K for 500 ps under the NVT ensemble (Andersen, 1980), followed by the NPT ensemble (Andersen, 1980; Berendsen et al., 1984) at 300 K and 1 atm for 1 ns. The unit cell dimensions and density of the amorphous HDPE after the relaxation were 4.98 × 9.93 × 8.15 nm^3 and 0.983 g/cm^3, respectively.

A graphite block consisting of 13-layer stacked graphene was also prepared. The x-y plane dimension of the graphite block model was determined to be 4.2 × 8.6 nm^2, which was closest to the size of the amorphous HDPE model.

Oxygen bonding treatment on rCF surface

The main purpose of the present simulation was to quantify the influence of surface reformation of the graphite block with respect to the existence of the oxygen functional groups induced by the IPL irradiation (Cassagneau et al., 2000; Hontoria-Lucas et al., 1995; Shin et al., 2009). Accordingly, molecular structures of graphite with oxygen coverage (OC; defined as the ratio of the number of oxygen atoms to that of the carbon atoms at the surface of graphite) of 0%, 2%, 4%, 6%, 8%, and 10% were considered in succession. The oxygen functional group of carbon allotropy is mainly composed of epoxide and hydroxyl groups (Lerf et al., 1997; He et al., 1992); the composition of the functional group depends on the cohesive and formation energies of the functional group pairs (Fonseca et al., 2015; Yan and Chou, 2010; Lahaye et al., 2009). The formation energy of the isolated functional groups with a 1:1 hydroxyl-to-epoxide ratio is the lowest (Yan and Chou, 2010); thus, it is the most favorable configuration of the GO molecular structure. Therefore, a 1:1 hydroxyl-to-epoxide ratio was considered for all GOs in the MD modeling process.

When the graphite surface was exposed to light irradiation, the OC of the outermost graphene layer increased preferentially until it was fully oxidized and exfoliated, which led to the oxidation of the subsequent graphene layer (Lee et al., 1999; Boukhvalov, 2014). Thus, oxygen atoms were randomly distributed

over the graphite surface with an interval of 1.46 Å, which was the average C-O bond length of the epoxide (1.43 Å) and hydroxyl (1.49 Å) functional groups (Elias et al., 2009; Boukhvalov et al., 2008). As the functional group was formed, the bonding type of carbon atoms involved in the reaction changed from sp^2 to sp^3 (Yan and Chou, 2010; Lee et al., 1999; Elias et al., 2009). To describe these chemical and structural changes in the MD simulation, firstly, the molecular structure of the graphite block was equilibrated at 300 K for 500 ps under the NVT (canonical) ensemble. Following the relaxation procedure, additional equilibration runs were performed under the same thermodynamic ensemble for the graphite oxide (GO) models, in which the epoxide and hydroxyl groups were generated on the outermost graphene layers. The equilibrated molecular structures of the graphite and GO models are shown in Figure S9.

Pull-out simulation of HDPE/GO bilayer system

The amorphous HDPE and individual GO with different OC models were merged in the z-direction, while preserving their periodicity. Then, a potential energy minimization using a conjugate-gradient method, NVT ensemble equilibration at 300 K for 500 ps, and NPT ensemble equilibration at 300 K and 1 atm for 1 ns, were carried out sequentially, to obtain a thermally relaxed configuration of the bilayer system. The detailed geometries of the models considered are summarized in Table S2 (also refer to Figure S10A). To quantitatively estimate the effect of OC on the interfacial shear strength at the HDPE/GO interface, the pull-out test environment of the GO from the HDPE matrix was set up as shown in Figure S10B. A large vacuum slab with a length of 20 nm in the y-direction was inserted on the right side of the HDPE/GO model while all the atoms in the 0.4-nm region at both ends of the model were fully constrained. As the periodicity in the y-direction was necessarily broken, the carbon atoms of the GO at the ends of the unit cell in the y-direction were dangled by the hydrogen atoms. An additional relaxation process under the NVT ensemble at 0.1 K for 100 ps was performed. Then, the GO layer was pulled out at a velocity of 1.0 Å/ps in the y-direction until the GO completely escaped from the matrix region and it no longer had an interatomic interaction force. The quasi-static pull-out process of the 6%-OC GO block is shown as a representative example in Figure S11. A polymer consistent force field (Sun et al., 1994) was applied to calculate all the atomic interactions in the model. The modeling of the HDPE/GO bilayer system and its equilibration MD run were conducted using Materials Studio® software from Dassault Systems. The pull-out tests were conducted using a Large-scale Atomic/Molecular Massively Parallel Simulator (LAMMPS) (Plimpton, 1995).

Molecular scale interlocking: Characterization and quantification

The adhesion force and IFSS at the interface between the graphite block and HDPE were strongly dependent on the physical interlocking conditions. To evaluate the physical interlocking by the surface groove at a molecular scale, the root-mean-square surface roughness (R_q) of the thermally relaxed interface between the graphite block and HDPE surfaces, modeled by the MD simulation was calculated as follows:

$$R_q = \sqrt{\frac{L}{a}\sum_{k=1}^{n}(z_k - \bar{z})^2} \qquad \text{(Equation 9)}$$

where n is the number of sampling data; z_i is the roughness irregularities from the mean height z; and L is the length of the contact interface along the x-direction. The measuring scale a is the minimum dimension (2.7 Å in this study), at which the averaged position of the surface atoms in the z-direction was measured as the effective height of the surface. As shown in Figure S12, as the OC increased, the surface roughness of the graphite block increased, and reached the same order of roughness as that of the HDPE surfaces. The surface of graphite with almost no roughness gradually deteriorates with increasing OC. In contrast, the amorphous HDPE surface inherently possesses molecular-scale surface roughness owing to the surface morphology of the polymer. Mechanical interlocking improves when the molecular-scale roughness of the two components in the interfacial region is similar (Lim et al., 2022). In other words, the flatness of the graphite surfaces decreases as the functional groups are attached, creating a strongly coupled interface with HDPE.

From an energy standpoint, the strong, non-bonded interactions between the atoms on the GO and HDPE surfaces also played a major role. Because the interfacial region considered in this study experienced only van der Waals interactions described by the Lennard–Jones potential, the depth of the potential well had a strong correlation to the attraction force at the interface (Zhao et al., 2021; Chen et al., 2017; Wernik et al., 2012). The increased number density of the GO oxygen and HDPE carbon pair resulted in the deepest potential well and formed strong, non-bonded interactions. These interactions induce GO layer deformation

on the HDPE surface, resulting in the intrinsic molecular-scale roughness of GO in HDPE. The structural compatibility between the GO and HDPE surfaces was considerably enhanced as the number density of the functional groups increased, creating a strongly coupled interface. Figure S13 shows the non-bonding potential energy functions of the interatomic pair, consisting of GO and HDPE. The molecular interactions in the interfacial region were dominated by the 9-6 Lennard–Jones potential (V_{LJ}) as follows:

$$V_{LJ} = 4\varepsilon_{\alpha\alpha}\left[\left(\frac{r_{\alpha\alpha}}{r}\right)^9 - \left(\frac{r_{\alpha\alpha}}{r}\right)^6\right] \quad \text{(Equation 10)}$$

where $\varepsilon_{\alpha\alpha}$ and r are the depth of the potential well and the distance between two α atoms, respectively, and $r_{\alpha\alpha}$ is the finite distance at which the interpair potential becomes zero. By applying the Lorentz-Berthelot combining rule, the non-bonded potential parameters between different atom species α and β can be defined as $r_{\alpha\beta} = \frac{r_{\alpha\alpha}+r_{\beta\beta}}{2}$ and $\varepsilon_{\alpha\beta} = \frac{\varepsilon_{\alpha\alpha}+\varepsilon_{\beta\beta}}{2}$, respectively. The oxygen atom from the hydroxyl group (''oh'') and the one from the epoxide group (''o3e'') use the same non-bond interaction parameters ($r_{\alpha\alpha}$ =3.535 Å and $\varepsilon_{\alpha\alpha}$ = 0.24 kcal/mol); thus, they are energetically equivalent. Figure S13B indicates that the potential well was the deepest for the hydroxyl/epoxide oxygen and HDPE carbon pairs. Such a significant depth of the potential well is strongly correlated to the attraction force at the interface (Wernik et al., 2012; Yang et al., 2021).

The potential well was the deepest for the functional group oxygen (o3e) and HDPE carbon (c3) pair. Herein, the ''o3e-c3'' pair is related to the binding energy between the oxygen and carbon atoms observed by XPS, as shown in Figure 1C. The oxygen atoms created on the rCF surface upon IPL irradiation undergo strong, non-bonded interactions with the carbon atoms of the neighboring polymer chains, enhancing the molecular-scale contact and explaining why the concentration of O-C pairs on the rCF surface coincides with the trend of IFSS shown in Figure 2A.

During the pull-out process of the GO block with a fixed displacement, the internal force acting on the GO block and its maximum value were measured to evaluate the interfacial friction between the GO and HDPE surfaces, as shown in Figures S14 and 3C. The internal force decreased from a maximum value as the interface area between the GO and HDPE surfaces decreased. The monotonic increase in not only the peak of the internal force, but also the IFSS was clearly observed, as the OC increased. The physical interlocking by functional groups restricted the sliding between the GO and HDPE surfaces, for which a higher external force was required to shear the interface. Therefore, modification of the graphite surface by oxygen-containing functional groups reinforces the interfacial adhesion characteristics. It is also worth noting that the results of the change in the roughness characteristics by the oxygen functional group agreed very well with those reported in the literature (Brewis and Briggs, 1981).

Calculation of atomic stress distribution

To further discuss the enhancement of the IFSS, we calculated the atomic stress tensor for every atom in the bilayer system as follows (Heyes, 1994):

$$\sigma_{ij} = \frac{1}{\overline{V}}\left(-\sum_i^N m_i(v_i \times v_i) + \frac{1}{2}\sum_i^N\sum_{j\neq i}^N r_{ij} \times F_{ij}\right) \quad \text{(Equation 11)}$$

where N is the number of atoms in the system volume V; m_i and v_i are the mass and velocity of the i^{th} atom; and r_{ij} and F_{ij} are the distance and interaction between the i^{th} and j^{th} atoms, respectively. The volume of single atoms on the upper surface of the GO was calculated using the Voronoi tessellation method.

As shown in Figures 3D and S15, a local concentration of stress was clearly observed, especially near the oxygen groups. The area, where the compressive stresses existed, contained notches, which resulted in a higher tensile stress distribution on the graphite surface. Furthermore, the tensile stress of the GO surface in the x-direction was not uniformly distributed, but accumulated on the opposite side of the pull position.

Classification of interactions according to oxygen functional groups

The comparison of the effects according to the type of oxygen functional group is of great interest. The oxygen atom of the hydroxyl group has higher mobility than the epoxide group, which forms strong, triangular bonds. Although hydroxyl group oxygen and epoxide group oxygen have the same non-bond interaction parameters, the structural diversity at the molecular scale can affect the mechanical stress of each

group during pull-out simulations (Brewis and Briggs, 1981; Gao et al., 2011). As shown in Figure 3F, we considered virtual spherical regions of 3 Å radius with the centers located at the oxygen atoms. The regions were classified into epoxide and hydroxyl groups, according to the type of bond formed by the central oxygen atom. The σ_{xx} components inside each region were averaged at a pull-out displacement of 20 Å. The results are in line with the observations reported in the literature that the reactivity of the hydroxyl group was more than 1.5 times higher than that of the epoxide group owing to the strong interaction with tailored hydrogen bonds (Shin et al., 2009; Lerf et al., 1997; He et al., 1992; Vinod et al., 2018; Ghaderi and Peressi, 2010). Therefore, the present results allow the understanding of a fundamental mechanism for evaluating the physical attributes to be considered by the IPL process for enhancing the IFSS of GO. IPL process optimization studies for the selective increase in the number density of hydroxyl groups are required for future work.